# Synthesis and Characterization of Mixed Phthalocyaninato and *meso*-Tetrakis(4-chlorophenyl)porphyrinato Triple-Decker Complexes – Revealing the Origin of Their Electronic Absorptions

**Xuan Sun,[a] Renjie Li,[a] Daqi Wang,[b] Jianmin Dou,[b] Peihua Zhu,[a] Fanli Lu,[a] Changqin Ma,[a] Chi-Fung Choi,[c] Diana Y. Y. Cheng,[c] Dennis K. P. Ng,[c] Nagao Kobayashi,[d] and Jianzhuang Jiang*[a]**

**Keywords:** Phthalocyanines / Porphyrins / Rare earth metals / Sandwich complexes / Triple-decker complexes

Two series of mixed phthalocyaninato and porphyrinato rare earth(III) triple-decker complexes $[M_2(Pc)(TClPP)_2]$ (**1a–10a**) and $[M_2(Pc)_2(TClPP)]$ (**1b–11b**) [M = Y, La–Er except Ce and Pm; Pc = phthalocyaninate; TClPP = tetrakis(4-chlorophenyl)-porphyrinate] have been prepared by treating the half-sandwich complexes [M(TClPP)(acac)] (acac = acetylacetonate), generated in situ from $[M(acac)_3]\cdot nH_2O$ and $H_2(TClPP)$, with $Li_2(Pc)$. All the triple-decker complexes have been characterized by a wide range of spectroscopic and electrochemical methods. The molecular structures of $[M_2(Pc)(TClPP)_2]$ (M = Y, Ho) have also been determined, and show a symmetrical disposition of ligands, with two outer domed TClPP and one inner Pc rings. A systematic investigation of the optical and electrochemical data of these complexes has revealed the nature of the HOMO and LUMO, as well as the origin of the electronic absorptions of these triple-decker complexes.


## Introduction

Triple-decker rare-earth complexes with mixed phthalocyaninato and porphyrinato ligands have received considerable attention.[1] With two different classes of macrocyclic ligands, which can be arranged in different order in the complexes, this exotic class of compounds exhibits intriguing spectroscopic and electrochemical properties that cannot be found in non-sandwich counterparts. Owing to the high stability, the presence of multiple redox states, and the ability to store charge for a significant period of time, these triple-decker complexes are promising molecular-based materials for information-storage devices such as multistate counters and molecular capacitors.[2] Despite these important applications and other intrinsic interest in the structural and spectroscopic aspects, heteroleptic triple-deckers with these tetrapyrrole ligands remain rare and are confined to a number of lanthanides.[2–4] As part of our continuing interest in heteroleptic rare-earth complexes with tetrapyrrole ligands,[1,4] we describe herein a systematic study of two series of phthalocyaninato and porphyrinato triple-decker complexes, namely $[M_2(Pc)(TClPP)_2]$ (M = Y, La–Ho except Ce and Pm) and $[M_2(Pc)_2(TClPP)]$ (M = Y, La–Er except Ce and Pm), including their synthesis, spectroscopic and structural characterization, and electrochemical properties. A detailed examination of these properties has led to a better understanding of their electronic structure as well as the origin of the electronic transitions of these complexes.

## Results and Discussion

### Synthesis and Characterization

According to our previously described procedure,[4a,4b] treatment of [M(TClPP)(acac)] (M = Y, La–Er except Ce and Pm), generated in situ from $[M(acac)_3]\cdot nH_2O$ and $H_2(TClPP)$, with $Li_2(Pc)$ gave a mixture of the triple-deckers $[M_2(Pc)(TClPP)_2]$ and $[M_2(Pc)_2(TClPP)]$, which could be separated readily by column chromatography (Figure 1). The yields for both series of complexes {5–48% for $[M_2(Pc)(TClPP)_2]$ and 4–40% for $[M_2(Pc)_2(TClPP)]$} were higher for lanthanides with a moderate size, while both

[a] Department of Chemistry, Shandong University
Jinan 250100, China
Fax: (internat.) + 86-531-856-5211
E-mail: jzjiang@sdu.edu.cn
[b] Department of Chemistry, Liaocheng University
Liaocheng 252000, China
[c] Department of Chemistry, The Chinese University of Hong Kong
Shatin, N.T., Hong Kong, China
[d] Department of Chemistry, Graduate School of Science, Tohoku University
Sendai 980-8578, Japan
Supporting information for this article is available on the WWW under http://www.eurjic.org or from the author.

  **DOI: 10.1002/ejic.200400289** 

early and late lanthanide analogues gave a lower yield (Tables S1 and S2, and Figure S1 in the Supporting Information). Attempts to isolate the late lanthanide complexes $[M_2(Pc)(TClPP)_2]$ (M = Er−Lu) and $[M_2(Pc)_2(TClPP)]$ (M = Tm−Lu) were not successful. Apparently, mid-lanthanides have an appropriate size to optimize the separation of the three ligands so that they are close enough to maximize the stabilization due to π-π interactions yet the axial compression of the π-systems remains tolerable. This balance leads to a higher stability and therefore a higher yield of the complexes.

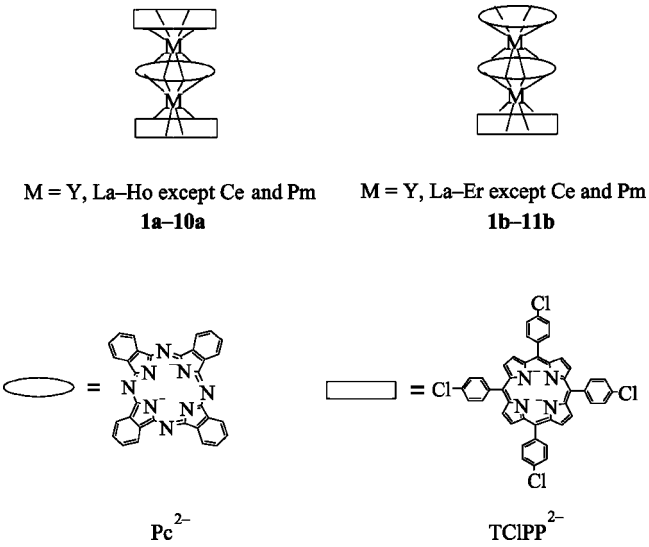


Figure 1. Schematic structures of the mixed-ring rare-earth triple-decker complexes with phthalocyaninato and *meso*-tetrakis(4-chlorophenyl)porphyrinato ligands

Except for a few early lanthanide triple-deckers, which are not very stable even in the solid state, all the triple-deckers gave satisfactory elemental analysis results (Tables S1 and S2). Intense molecular ion (or protonated molecular ion) peaks with expected isotopic patterns were also observed in the MALDI-TOF mass spectra for all these complexes. The mass spectroscopic data are also summarized in Tables S1 and S2, and a partial MALDI-TOF spectrum of $[Tb_2(Pc)(TClPP)_2]$ (**7a**) showing the isotopic distribution of the protonated molecular ion and the corresponding simulated spectrum is given in the Supporting Information (Figure S2) as an example.

Table 1 collects the $^1H$ NMR spectroscopic data of the triple-deckers $[M_2(Pc)(TClPP)_2]$ [M = Sm (**4a**), Y (**9a**)] and $[M_2(Pc)_2(TClPP)]$ [M = Sm (**4b**), Y (**9b**)] in $CDCl_3$. The spectral assignment could easily be made on the basis of the integration and multiplicity of the signals, and with reference to the previous results for the Eu analogues **5a** and **5b**,[4b] and the triple-deckers $[M_2(Pc)(TPyP)_2]$ [M = La, Eu; TPyP = *meso*-tetrakis(4-pyridyl)porphyrinate].[4f] Satisfactory NMR spectroscopic data, however, could not be obtained for the other triple-deckers due to the highly paramagnetic character of the metal centers.

### Electronic Absorption Spectra

The electronic absorption spectra for both series of triple-decker complexes **1a**−**10a** and **1b**−**11b**, were measured in $CHCl_3$ and the data are compiled in Tables 2 and 3. Figures 2 and 3 display the spectra for $[M_2(Pc)(TClPP)_2]$ and $[M_2(Pc)_2(TClPP)]$ (M = Nd, Gd, Dy), respectively, as examples. For the first series of complexes, the Pc Soret band at 354−360 nm shifts slightly to the blue, while the Q-band absorptions at 485−494, 548−573, and 876−997 nm are all red-shifted due to the lanthanide contraction (Table 2). The TClPP Soret band at 418−420 nm and the remaining Q band at 606−608 nm remain relatively unshifted for the whole series of complexes.

Some of the absorption bands of **1b**−**11b** are also dependent on the size of the metal centers. As shown in Table 3, the TClPP Soret band at 411−418 nm and the longest-

Table 1. $^1H$ NMR spectroscopic data (δ) for the triple-deckers $[M_2(Pc)(TClPP)_2]$ (M = Sm, Y) and $[M_2(Pc)_2(TClPP)]$ (M = Sm, Y) in $CDCl_3$

| Compound | Pc-$H_\alpha$ | Pc-$H_\beta$ | TClPP-$H_\beta$ | TClPP-$H_{aryl}$ |
|---|---|---|---|---|
| $[Sm_2(Pc)(TClPP)_2]$ (**4a**) | 8.10−8.18 (m, 8 H) | 7.81−7.84 (m, 8 H) | 6.67 (s, 16 H) | 7.57 (dd, *J* = 1.8, 8.1 Hz, 8 H)<br>7.38 (dd, *J* = 1.8, 8.1 Hz, 8 H)<br>7.10 (dd, *J* = 1.8, 8.1 Hz, 8 H)<br>6.61 (dd, *J* = 1.8, 8.1 Hz, 8 H) |
| $[Y_2(Pc)(TClPP)_2]$ (**9a**) | 9.46−9.49 (m, 8 H) | 8.55−8.58 (m, 8 H) | 7.29 (s, 16 H) | 8.34 (dd, *J* = 2.1, 8.1 Hz, 8 H)<br>7.98 (dd, *J* = 2.1, 8.1 Hz, 8 H)<br>6.96 (dd, *J* = 2.1, 8.1 Hz, 8 H)<br>5.86 (dd, *J* = 2.1, 8.1 Hz, 8 H) |
| $[Sm_2(Pc)_2(TClPP)]$ (**4b**) | 7.93−7.95 (m, 8 H)<br>7.83−7.86 (m, 8 H) | 7.71−7.74 (m, 8 H)<br>7.65−7.68 (m, 8 H) | 6.60 (s, 8 H) | 7.90 (dd, *J* = 2.1, 8.1 Hz, 4 H)<br>7.88 (dd, *J* = 2.1, 8.1 Hz, 4 H)<br>7.13 (dd, *J* = 2.1, 8.1 Hz, 4 H)<br>6.78 (dd, *J* = 2.1, 8.1 Hz, 4 H) |
| $[Y_2(Pc)_2(TClPP)]$ (**9b**) | 9.11−9.20 (m, 8 H)<br>8.48−8.59 (m, 8 H) | 8.68−8.73 (m, 8 H)<br>8.05−8.12 (m, 8 H) | 7.33 (s, 8 H) | 8.48−8.59 (overlapped with one of the Pc-$H_\alpha$ multiplets)<br>8.02 (dd, *J* = 2.1, 8.1 Hz, 4 H)<br>6.98 (dd, *J* = 2.1, 8.1 Hz, 4 H)<br>5.98 (dd, *J* = 2.1, 8.1 Hz, 4 H) |

  

Table 2. Electronic absorption data for **1a**−**10a** in $CHCl_3$

| Compound | $\lambda_{max}$ [nm] (log $\varepsilon$) | | | | | |
|---|---|---|---|---|---|---|
| **1a** | 360 (5.01) | 420 (5.45) | 485 (4.43) | 551 (4.28) | 608 (4.30) | 876 (3.86) |
| **2a** | 360 (4.99) | 420 (5.38) | 489 (4.39) | 549 (4.15) | 607 (4.29) | 908 (3.83) |
| **3a** | 358 (4.94) | 420 (5.30) | 489 (4.44) | 548 (4.32) | 607 (4.25) | 919 (4.10) |
| **4a** | 355 (4.96) | 420 (5.27) | 492 (4.49) | 556 (4.40) | 606 (4.29) | 937 (3.96) |
| **5a** | 354 (5.04) | 419 (5.32) | 492 (4.57) | 559 (4.15) | 605 (4.34) | 950 (3.94) |
| **6a** | 354 (5.05) | 419 (5.36) | 493 (4.55) | 563 (4.05) | 606 (4.24) | 955 (4.04) |
| **7a** | 354 (5.02) | 419 (5.33) | 494 (4.53) | 565 (4.17) | 606 (4.19) | 973 (3.94) |
| **8a** | 354 (5.10) | 419 (5.38) | 494 (4.64) | 567 (4.20) | 606 (4.30) | 987 (3.89) |
| **9a** | 354 (5.10) | 418 (5.34) | 494 (4.68) | 566 (4.16) | 607 (4.39) | 995 (3.80) |
| **10a** | 354 (5.09) | 418 (5.33) | 494 (4.68) | 573 (4.18) | 606 (4.40) | 997 (3.77) |

Table 3. Electronic absorption data for **1b**−**11b** in $CHCl_3$

| Compound | $\lambda_{max}$ [nm] (log $\varepsilon$) | | | | | | |
|---|---|---|---|---|---|---|---|
| **1b** | 342 (5.21) | 418 (4.94) | | | | 616 (4.86) | 689 (4.55) |
| **2b** | 342 (5.14) | 418 (5.08) | 489 (4.43) | | 553 (4.36) | 619 (4.75) | 694 (4.61) |
| **3b** | 342 (5.18) | 417 (5.11) | 489 (4.33) | 524 (4.42) | 556 (4.37) | 617 (4.81) | 705 (4.63) |
| **4b** | 343 (5.20) | 416 (5.03) | 491 (4.32) | 525 (4.47) | 560 (4.37) | 618 (4.87) | 720 (4.61) |
| **5b** | 342 (5.19) | 414 (5.05) | 491 (4.33) | 521 (4.42) | 557 (4.36) | 617 (4.84) | 723 (4.55) |
| **6b** | 343 (5.22) | 413 (5.03) | 493 (4.32) | 524 (4.40) | 564 (4.37) | 618 (4.84) | 731 (4.50) |
| **7b** | 343 (5.21) | 413 (5.01) | | 523 (4.39) | | 618 (4.81) | 737 (4.45) |
| **8b** | 343 (5.19) | 413 (4.98) | | 524 (4.37) | | 619 (4.76) | 744 (4.39) |
| **9b** | 343 (5.19) | 412 (4.95) | | 523 (4.35) | | 618 (4.74) | 747 (4.35) |
| **10b** | 343 (5.17) | 411 (4.94) | | 522 (4.34) | | 618 (4.71) | 751 (4.31) |
| **11b** | 343 (5.17) | 412 (4.95) | | 521 (4.45) | | 617 (4.72) | 757 (4.42) |

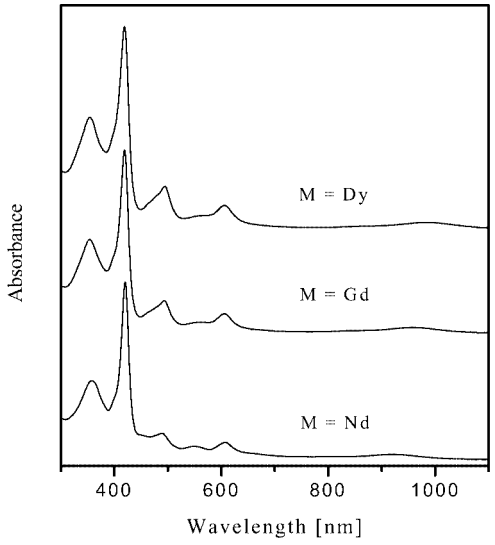


Figure 2. Electronic absorption spectra of $[M_2(Pc)(TClPP)_2]$ (M = Nd, Gd, Dy) in $CHCl_3$

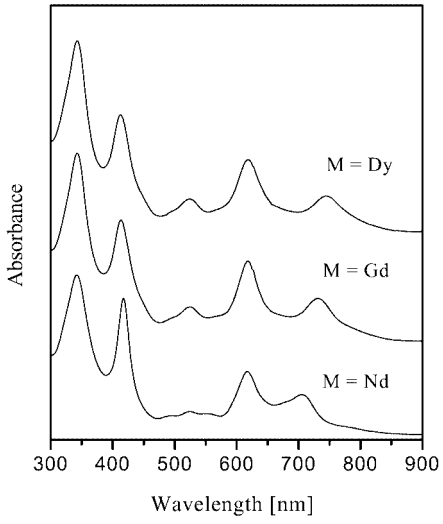


Figure 3. Electronic absorption spectra of $[M_2(Pc)_2(TClPP)]$ (M = Nd, Gd, Dy) in $CHCl_3$

wavelength Q-band at 689−757 nm are shifted to the blue and red, respectively, across the lanthanide series. For this series of complexes, the positions of the Pc Soret band (342−343 nm) and the other Q-bands in the visible region are not very sensitive to the metal centers.

In the mixed-ring triple-deckers $[M_2(Pc)(TClPP)_2]$ (**1a**−**10a**) and $[M_2(Pc)_2(TClPP)]$ (**1b**−**11b**), the close proximity of the three conjugated π-systems in a face-to-face configuration induces a splitting of the monomer (Pc and TClPP) molecular orbitals. As shown in Figure 4, the interactions of the doubly degenerate $e_g$ LUMO of both ligands, the $a_{1u}$ HOMO of Pc, and the $a_{1u}$ second HOMO of TClPP result in the formation of three doubly degenerate lowest-unoccupied molecular orbitals (the bonding LUMO, second non-bonding LUMO, and third anti-bonding LUMO) and three non-degenerate highest-occupied molecular orbitals (the third bonding HOMO, second non-bonding

  

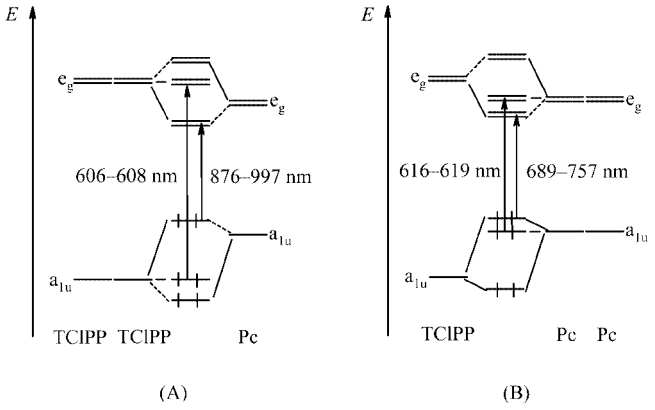


Figure 4. Partial molecular-orbital diagrams for $[M_2(Pc)(TClPP)_2]$ (A) and $[M_2(Pc)_2(TClPP)]$ (B)

HOMO, and first anti-bonding HOMO).[5] Due to the intrinsic difference in the electronic structure, the $a_{1u}$ orbital of Pc is higher in energy than that of TClPP, while the $e_g$ orbitals of Pc are lower than those of TClPP. Therefore, for both series of triple-deckers, the first anti-bonding HOMO and the first bonding LUMO are mainly from the phthalocyaninato ligand(s), whereas the third bonding HOMO and third anti-bonding LUMO have higher porphyrin character. The second non-bonding HOMO and non-bonding LUMO are pure TClPP and Pc orbitals, respectively, for $[M_2(Pc)(TClPP)_2]$ (**1a**−**10a**) and $[M_2(Pc)_2(TClPP)]$ (**1b**−**11b**). Along with the lanthanide contraction, the ring-to-ring interactions increase, resulting in an increase in the splitting between the first and second HOMOs as well as the second and third HOMOs of the triple-deckers. This simplified bonding picture can be used to interpret the electronic absorption data of these triple-decker complexes. For both series of complexes, the lowest-energy absorption band can be attributed to the electronic transition from the anti-bonding HOMO to the bonding LUMO, which is red-shifted across the lanthanide series (Tables 2 and 3). The second-lowest-energy absorption band can be ascribed to the transition from the second non-bonding HOMO to the second non-bonding LUMO, which remains essentially unchanged for the whole lanthanide series. Similarly, the Soret bands at 418−420 nm for $[M_2(Pc)(TClPP)_2]$ (**1a**−**10a**) and 342−345 nm for $[M_2(Pc)_2(TClPP)]$ (**1b**−**11b**) should also involve non-bonding orbitals with a pure TClPP or Pc character, respectively. It is worth noting that the dependence of the other Soret bands at 354−360 nm for $[M_2(Pc)(TClPP)_2]$ (**1a**−**10a**) and 412−418 nm for $[M_2(Pc)(TClPP)_2]$ (**1b**−**11b**) on the rare-earth ionic size clearly indicates the mixed phthalocyanine and porphyrin character of these transitions, suggesting the contributions from both porphyrin and phthalocyanine ligands to the molecular orbitals involved in these transitions.

## IR Spectra

IR spectroscopy is a useful tool to reveal the nature of phthalocyaninato ligands in their rare-earth sandwich complexes. The IR characteristics of several series of double- and triple-decker phthalocyaninato and/or porphyrinato rare-earth compounds, namely $[M(Pc')_2]$, $[M(Pc')(Por)]$, $[M_2(Pc')(Por)_2]$, and $[M_2(Pc')_2(Por)]$ (Pc′ = general phthalocyaninate; Por = general porphyrinate) have been systematically studied.[6] An intense band at 1312−1323 $cm^{-1}$ has been observed for neutral bis(phthalocyaninato) and mixed (phthalocyaninato)(porphyrinato) rare earth(III) double-decker complexes. This can be attributed to the $Pc^{\cdot-}$ IR marker band. On the other hand, a moderately strong band at ca. 1329 $cm^{-1}$ has been observed for $[Ce^{IV}(Pc)_2]$ and $[M_2(Pc)_2\{Pc(OC_8H_{17})_8\}]$ $[Pc(OC_8H_{17})_8$ = 2,3,9,10,16,17,23,24-octaoctyloxyphthalocyaninate], which contain dianionic phthalocyanine rings. This band is therefore regarded as the characteristic IR band for $Pc^{2-}$.[6] For the present two series of complexes, the dianionic nature of the phthalocyaninato ligand(s) was unambiguously verified by the observation of the characteristic $Pc^{2-}$ IR band at ca. 1330 $cm^{-1}$. As expected, the relative intensity of this band is higher for **1b**−**11b** than for **1a**−**10a** due to the higher Pc/TClPP ratio.

## Structural Studies of $[M_2(Pc)(TClPP)_2]$ (M = Y, Ho)

The molecular structures of $[M_2(Pc)(TClPP)_2]$ [M = Y (**9a**), Ho (**10a**)] were determined by X-ray diffraction analysis. Both compounds are isostructural and crystallize in the same tetragonal system with a *P*4/*n* space group together with a disordered $CH_2Cl_2$ molecule. It is worth noting that structurally characterized mixed-ring triple-deckers remain rare so far, and to the best of our knowledge they are limited to [(TPP)Ce(Pc)Gd(OEP)] (TPP = *meso*-tetraphenylporphyrinate; OEP = octaethylporphyrinate),[7] $[Ce_2(Pc)_2(TOMePP)]$ [TOMePP = *meso*-tetrakis(4-methoxyphenyl)porphyrinate],[8] $[Ce_2\{Pc(OMe)_8\}(TPP)_2]$ [Pc-$(OMe)_8$ = 2,3,9,10,16,17,23,24-octamethoxyphthalocyaninate],[8] $[Nd_2(Pc)_2(TOMePP)]$,[9] and $[Nd_2(Nc)(OEP)_2]$ (Nc = naphthalocyaninate).[4d]

Figure 5 shows the molecular structure of $[Ho_2(Pc)(TClPP)_2]$ (**10a**) in two different perspective views. Each holmium center is octa-coordinated by the pyrrole and isoindole nitrogen atoms of an outer TClPP and the central Pc rings, respectively, confirming the arrangement of ligands as [(TClPP)Ho(Pc)Ho(TClPP)]. The two holmium centers, however, are not identical in terms of their coordination geometry and separation from the ligands. The Ho1 atom adopts a slightly distorted square-antiprismatic structure while the Ho2 atom exhibits a slightly distorted cubic geometry. The Pc ring is slightly domed toward the Ho2 atom. Both holmium centers lie closer to the TClPP ring due to its larger central cavity compared with the Pc ligand (1.131 vs. 2.004 Å for Ho1; 1.218 vs. 1.687 Å for Ho2), and are not equidistant from the TClPP and Pc ligands. These structural features are clearly different from those revealed in the triple-deckers $[Ce_2\{Pc(OMe)_8\}(TPP)_2]$[8] and $[Nd_2(Nc)(OEP)_2]$,[4d] which are centrosymmetric and have two identical metal environments. This could be attributed to the different crystal packing forces for these complexes.

  

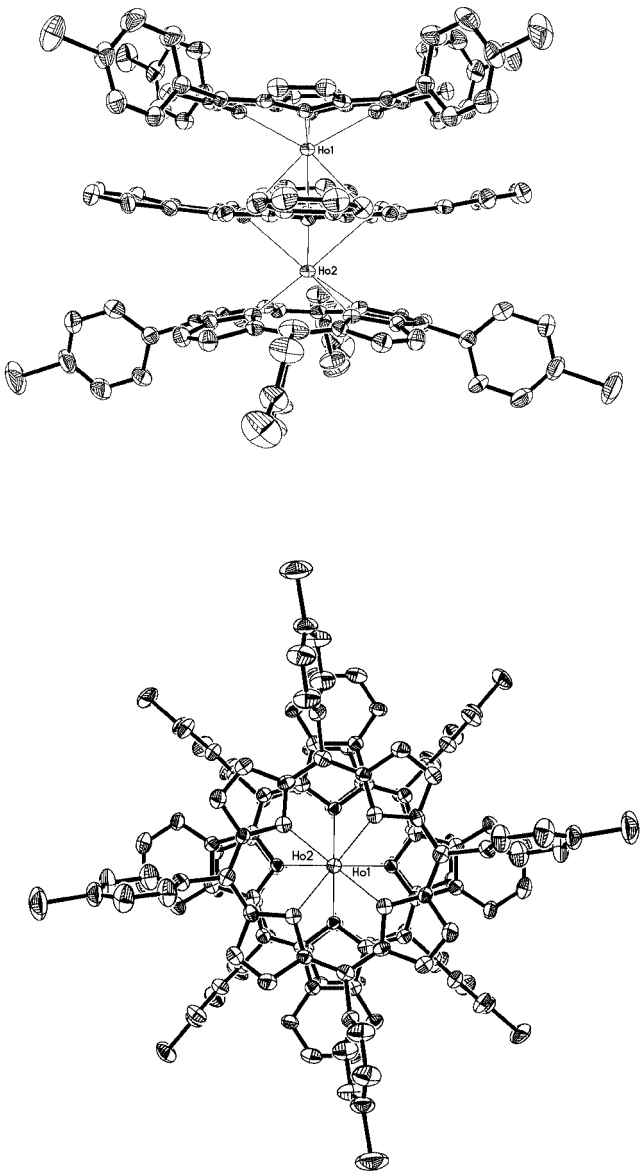


Figure 5. Molecular structure of $[Ho_2(Pc)(TClPP)_2]$ (**10a**) in two different perspective views; hydrogen atoms are omitted for clarity and the ellipsoids are drawn at the 30% probability level

## Electrochemistry

The redox behavior of the mixed-ring triple-deckers **1a**−**10a** and **2b**−**11b** was studied by cyclic voltammetry (CV) and differential pulse voltammetry (DPV) in $CH_2Cl_2$. Within the electrochemical window of $CH_2Cl_2$, five quasi-reversible one-electron oxidations and up to four quasi-reversible one-electron reductions were revealed for **1a**−**10a**. An additional reduction couple was observed for most of the triple-deckers in the series $[M_2(Pc)_2(TClPP)]$ (**3b**−**9b** and **11b**). The half-wave potentials for these two series of complexes are summarized in Tables 4 and 5. All these redox processes can be attributed to the successive removal of electrons from, or addition of electrons to, the ligand-based orbitals, as the oxidation state of the central trivalent rare-earth metals does not change. Figure 6 displays the cyclic and differential pulse voltammograms of **3a** and Figure 7 shows the variation of the redox potentials of **1a**−**10a** with the rare-earth ionic radii. It can be seen that the half-wave potentials of the first ($O^1$) and second ($O^2$) oxidation processes for **1a**−**10a**, which involve the removal of electrons from the HOMO, decrease linearly as the size of the metal center decreases. In contrast, the potentials of the other oxidation processes, including $O^3$ and $O^4$, which involve the second HOMO, remain virtually unchanged at 1.37−1.43 and 1.60−1.65 V (except **1a**). These results indicate that along with the lanthanide contraction, the HOMO increases in energy while the energy level of the second-highest occupied orbital remains relatively unchanged. This directly reveals the anti- and non-bonding nature for the HOMO and second HOMO and indirectly suggests the bonding nature for the third HOMO. All the reduction processes ($R^1$, $R^2$, $R^3$, and $R^4$) also appear to be insensitive to the size of the rare earth metal centers, suggesting that the energy level of the first (as well as the second and the third) lowest unoccupied orbital remains relatively constant for the whole series. Therefore, the energy separation between the HOMO and the LUMO diminishes across the series, while that between the second-highest non-bonding occupied orbital and the second-lowest non-bonding unoccupied orbitals remains constant. The decrease in energy gap between the HOMO and LUMO is in agreement with the red-shift of the longest-wavelength near IR band at

Table 4. Half-wave redox potentials for **1a**−**10a** [V vs. SCE] in $CH_2Cl_2$ containing 0.1 M $[Bu_4N][ClO_4]$

| | $O^5$ | $O^4$ | $O^3$ | $O^2$ | $O^1$ | $R^1$ | $R^2$ | $R^3$ | $R^4$ | $\Delta E_{1/2}$ [a] |
|---|---|---|---|---|---|---|---|---|---|---|
| **1a** | +1.85[b] | +1.50 | +1.31 | +1.13 | +0.85 | −0.71 | −1.25 | −1.71[b] | | 1.56 |
| **2a** | +1.84 | +1.61 | +1.38 | +1.12 | +0.80 | −0.70 | −1.20 | −1.66 | −1.88[b] | 1.50 |
| **3a** | +1.85[b] | +1.61 | +1.37 | +1.12 | +0.78 | −0.70 | −1.21 | −1.67[b] | | 1.48 |
| **4a** | +1.85 | +1.65 | +1.41 | +1.09 | +0.73 | −0.72 | −1.23 | −1.69 | −1.89 | 1.45 |
| **5a** | +1.86[b] | +1.62 | +1.40 | +1.08 | +0.74 | −0.72 | −1.20 | −1.64 | | 1.46 |
| **6a** | +1.84 | +1.62 | +1.40 | +1.07 | +0.72 | −0.73 | −1.24 | −1.66 | −1.87[b] | 1.45 |
| **7a** | +1.85[b] | +1.65 | +1.42 | +1.05 | +0.67 | −0.73[b] | −1.29 | −1.67[b] | −1.96[b] | 1.40 |
| **8a** | +1.85[b] | +1.62 | +1.40 | +1.04 | +0.66 | −0.74 | −1.22 | −1.63 | −1.84[b] | 1.40 |
| **9a** | +1.82 | +1.63 | +1.41 | +1.03 | +0.65 | −0.74 | −1.21 | −1.65[b] | −1.90[b] | 1.39 |
| **10a** | +1.85[b] | +1.60 | +1.43 | +1.03 | +0.64 | −0.75 | −1.22 | −1.65[b] | −1.90[b] | 1.39 |

[a] $\Delta E_{1/2}$ is the potential difference between the first oxidation and the first reduction processes. [b] Recorded by DPV.

  

Table 5. Half-wave redox potentials for **1b**−**11b** [V vs. SCE] in $CH_2Cl_2$ containing 0.1 M $[Bu_4N][ClO_4]$

| | $O^5$ | $O^4$ | $O^3$ | $O^2$ | $O^1$ | $R^1$ | $R^2$ | $R^3$ | $R^4$ | $R^5$ | $\Delta E_{1/2}$ [a] |
|---|---|---|---|---|---|---|---|---|---|---|---|
| **2b** | +1.98[b] | +1.58 | +1.37 | +1.03 | +0.58 | −0.62 | −1.05[b] | −1.39[b] | | | 1.20 |
| **3b** | +1.95[b] | +1.60 | +1.34 | +1.00 | +0.54 | −0.66[b] | −1.12 | −1.51 | −1.72 | −2.01 | 1.20 |
| **4b** | +1.88 | +1.63 | +1.40 | +0.97 | +0.51 | −0.64 | −1.09 | −1.51 | −1.76[b] | −1.98[b] | 1.15 |
| **5b** | +2.00 | +1.63 | +1.42 | +0.94 | +0.47 | −0.63 | −1.11 | −1.50 | −1.57[b] | −1.92[b] | 1.10 |
| **6b** | +1.93 | +1.61 | +1.40 | +0.93 | +0.47 | −0.64 | −1.11 | −1.48 | −1.70[b] | −1.98[b] | 1.11 |
| **7b** | +1.93 | +1.61 | +1.41 | +0.91 | +0.44[b] | −0.65 | −1.09[b] | −1.52 | −1.76 | −1.98[b] | 1.09 |
| **8b** | +1.93 | +1.61 | +1.42 | +0.91 | +0.44[b] | −0.64 | −1.09 | −1.48 | −1.74 | −1.97[b] | 1.08 |
| **9b** | +2.00[b] | +1.62 | +1.41 | +0.89 | +0.43 | −0.69 | −1.07 | −1.56 | −1.69[b] | −1.95[b] | 1.12 |
| **10b** | +1.95 | +1.61 | +1.41 | +0.89 | +0.42 | −0.65 | −1.10 | −1.54 | −1.74[b] | | 1.07 |
| **11b** | +1.94 | +1.61 | +1.41 | +0.86 | +0.39 | −0.65 | −1.08 | −1.48 | −1.73[b] | −1.97[b] | 1.04 |

[a] $\Delta E_{1/2}$ is the potential difference between the first oxidation and the first reduction processes. [b] Recorded by DPV.

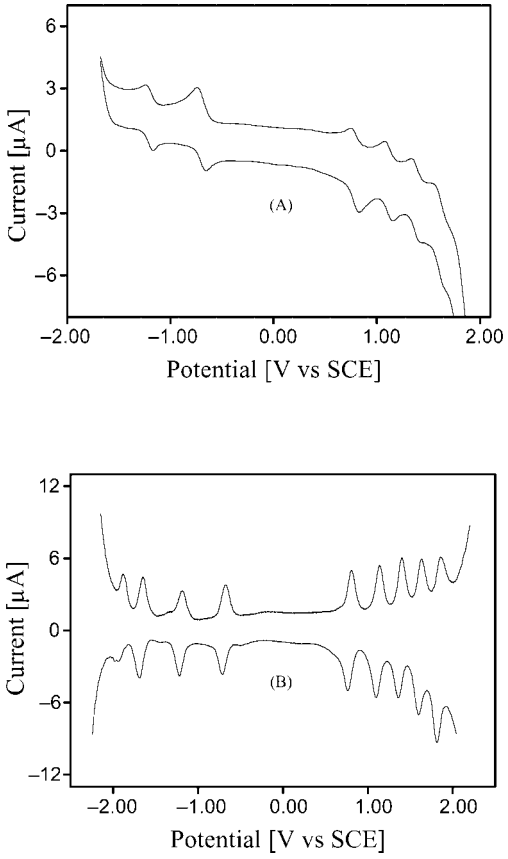


Figure 6. (A) Cyclic voltammogram and (B) differential pulse voltammogram of $[Nd_2(Pc)(TClPP)_2]$ (**3a**) in $CH_2Cl_2$ containing 0.1 M $[NBu_4][ClO_4]$ at a scan rate of 20 and 10 mV $s^{-1}$, respectively

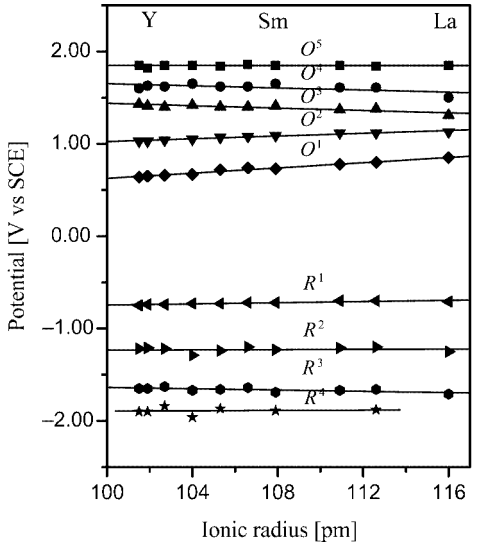


Figure 7. Plot of the half-wave potentials of the oxidation and reduction processes of $[M_2(Pc)(TClPP)_2]$ (**1a**−**10a**) as a function of the ionic radius of $M^{III}$

876−997 nm (Table 2). The main Q-band at 605−608 nm, which remains relatively unchanged for the whole series of complexes, can then be assigned to the electronic transition from the second-highest non-bonding occupied orbital to the second-lowest non-bonding unoccupied orbitals. The remaining weak Q-band at 551−573 nm is red-shifted as the size of the metal centers decreases (Table 2). This suggests that this absorption may arise from the electronic transition from the HOMO to the third-lowest unoccupied orbitals as the energy gap between these two sets of orbitals decreases across the series from La to Ho. Figure S3 (Supporting Information) compares the energy levels for the La (**1a**) and Ho (**10a**) triple-deckers.

The electrochemical behavior of $[M_2(Pc)_2(TClPP)]$ (**2b**−**11b**) is similar to that of $[M_2(Pc)(TClPP)_2]$ (**1a**−**10a**). Similar trends were observed for their redox potentials (Table 5) as a function of the ionic radius of the metal center. Thus, similar conclusions could be drawn about the frontier molecular orbitals and the corresponding electronic transitions for this series of complexes, except that the second-highest occupied orbitals and the second-lowest unoccupied orbitals are of pure Pc character instead of pure TClPP character in $[M_2(Pc)(TClPP)_2]$. By comparing the data in Tables 4 and 5, it can be seen that the $[M_2(Pc)_2(TClPP)]$ complexes undergo oxidation ($O^1$ and $O^2$) and reduction ($R^1$ and $R^2$) more readily than the corresponding $[M_2(Pc)(TClPP)_2]$ complexes.

As the first oxidation and the first reduction processes involve a one-electron transfer from the HOMO and to the LUMO of the molecule, respectively, the energy difference between these two redox processes, $\Delta E^\circ_{1/2}(O^1 - R^1)$, should reflect the energy required for the electronic transition from

  

the HOMO to the LUMO. This should therefore correlate with the lowest-energy electronic transition. As shown in Tables 4 and 5, the HOMO−LUMO gap for $[M_2(Pc)(TClPP)_2]$ (**1a**−**10a**) (1.39−1.56 V) is larger than that for $[M_2(Pc)_2(TClPP)]$ (**2b**−**11b**) (1.04−1.20 V). However, the lowest-energy electronic absorption band of **1a**−**10a** appears at longer wavelength than that of **2b**−**11b** due to the different ligand composition and ring-ring interaction in the two series. According to the electrochemical and absorption data for both series of triple-deckers tabulated in Tables 2−5, the equations $\Delta E^{\circ}_{1/2}(O^1 - R^1) - h\nu = -0.14$ (±0.02) and $\Delta E^{\circ}_{1/2}(O^1 - R^1) - h\nu = -0.58$ (±0.02) eV could be established for the series **a** and **b**, respectively, instead of the equation $\Delta E^{\circ}_{1/2}(O^1 - R^1) - h\nu = 0.01$ eV established for monomeric metalloporphyrins containing a pure porphyrin ligand.[10]

## Conclusions

Two series of mixed (phthalocyaninato)(porphyrinato) rare earth triple-decker complexes $[M_2(Pc)(TClPP)_2]$ and $[M_2(Pc)_2(TClPP)]$ have been prepared. All these compounds have been fully characterized with a wide range of spectroscopic and electrochemical techniques. The molecular structures of two triple-deckers $[M_2(Pc)(TClPP)_2]$ (M = Y, Ho) have also been determined. Systematic studies of the spectroscopic and electrochemical properties of both series of compounds reveal the nature of some frontier molecular orbitals and the electronic absorption bands of these complexes.

## Experimental Section

**General Remarks:** Anhydrous TCB (Aldrich) was used as received. Details regarding the treatment of the other solvents, preparation of the starting materials, and the instrumentation have been described previously.[11]

**General Procedure for the Preparation of $[M_2(Pc)(TClPP)_2]$ (1a−10a) and $[M_2(Pc)_2(TClPP)]$ (1b−11b):** A mixture of $H_2(TClPP)$ (75 mg, 0.10 mmol) and $[M(acac)_3]\cdot nH_2O$ (ca. 150 mg, 0.30 mmol) in TCB (20 mL) was refluxed under a slow stream of nitrogen for 4 h. The resulting dark cherry-red solution was cooled to room temperature, then $Li_2(Pc)$ (80 mg, 0.15 mmol) was added. The mixture was refluxed for a further 6 h, then the solvent was removed under reduced pressure. The violet-blue residue was chromatographed on a silica gel column using $CHCl_3$/hexanes (1:1) as eluent to give an olive-green band, which contained mainly the triple-decker $[M_2(Pc)(TClPP)_2]$, and a small amount of the double-decker $[M(Pc)(TClPP)]$ and unchanged $H_2(TClPP)$. After collecting this band, the column was further eluted with $CHCl_3$ to give a mixture of the triple-decker $[M_2(Pc)_2(TClPP)]$ and the double-decker $[M(Pc)_2]$. The triple-decker products were further purified by chromatography, followed by recrystallization from $CHCl_3$ and MeOH to give dark green or dark blue microcrystals of $[M_2(Pc)(TClPP)_2]$ and $[M_2(Pc)_2(TClPP)]$, respectively.

**X-ray Crystallographic Analysis of 9a and 10a:** Crystals suitable for X-ray diffraction analysis were grown by layering MeOH onto a $CH_2Cl_2$ solution of the compounds. Crystal data and details of data collection and structure refinement are given in Table 6. Data were collected with a Bruker SMART CCD diffractometer with an Mo-$K_\alpha$ sealed tube ($\lambda$ = 0.71073 Å) at 293 K, using the $\omega$-scan mode with an increment of 0.3°. Preliminary unit-cell parameters were obtained from 45 frames. Final unit-cell parameters were obtained by global refinements of reflections obtained from integration of all the frame data. The collected frames were integrated using the preliminary cell-orientation matrix. SMART software was used for collecting frames of data, indexing reflections, and determination of lattice constants; SAINT-PLUS for integration of intensity of reflections and scaling;[12] SADABS for absorption correction;[13] and SHELXL for space group and structure determination, refinements, graphics, and structure reporting.[14] CCDC-208839 (**9a**) and -208840 (**10a**) contain the supplementary crystallographic data for this paper. These data can be obtained free of charge at www.ccdc.cam.ac.uk/conts/retrieving.html [or from the Cambridge Crystallographic Data Centre, 12 Union Road, Cambridge CB2 1EZ, UK; Fax: (internat.) + 44-1223-336033; E-mail: deposit@ccdc.cam.ac.uk].

Table 6. Crystallographic data for **9a** and **10a**

| | **9a**·$CH_2Cl_2$ | **10a**·$CH_2Cl_2$ |
|---|---|---|
| Empirical formula | $C_{121}H_{66}Cl_{10}N_{16}Y_2$ | $C_{121}H_{66}Cl_{10}Ho_2N_{16}$ |
| Formula mass | 2276.22 | 2428.26 |
| Crystal size [mm] | 0.35 × 0.18 × 0.12 | 0.40 × 0.25 × 0.12 |
| Crystal system | tetragonal | tetragonal |
| Space group | *P*4/*n* | *P*4/*n* |
| *a* [Å] | 23.546 (16) | 23.437 (10) |
| *b* [Å] | 23.546 (16) | 23.437 (10) |
| *c* [Å] | 12.556 (12) | 12.580 (8) |
| *V* [Å] | 6961 (9) | 6910 (6) |
| *Z* | 2 | 2 |
| *F* (000) | 2304 | 2416 |
| $\rho_{calcd}$ [Mg m$^{-3}$] | 1.086 | 1.167 |
| $\mu$ [mm$^{-1}$] | 1.067 | 1.376 |
| θ range [°] | 2.52−25.00 | 2.75−25.00 |
| Reflections collected | 34772 | 34465 |
| Independent reflections | 6121 ($R_{int}$ = 0.1411) | 6081 ($R_{int}$ = 0.0844) |
| Parameters | 352 | 352 |
| $R1$ [$I > 2\sigma(I)$] | 0.0892 | 0.0633 |
| $wR2$ [$I > 2\sigma(I)$] | 0.2872 | 0.2182 |
| Goodness of fit | 1.014 | 1.010 |

## Acknowledgments

Financial support from the National Natural Science Foundation of China (Grant No. 20171028, 20325105), the National Ministry of Science and Technology of China (Grant No. 2001CB6105-04), the National Ministry of Education of China, and Shandong University for J. J., and The Chinese University of Hong Kong for D. K. P. N. is gratefully acknowledged.

[1] [1a] D. K. P. Ng, J. Jiang, *Chem. Soc. Rev.* **1997**, *26*, 433. [1b] J. Jiang, K. Kasuga, D. P. Arnold, in *Supramolecular Photosensitive and Electroactive Materials* (Ed.: H. S. Nalwa), Academic Press, New York, **2001**, pp. 113−210. [1c] J. Jiang, W. Liu, D. P. Arnold, *J. Porphyrins Phthalocyanines* **2003**, *7*, 459.
[2] [2a] J. Li, D. Gryko, R. B. Dabke, J. R. Diers, D. F. Bocian, W.

  

G. Kuhr, J. S. Lindsey, *J. Org. Chem.* **2000**, *65*, 7379. [2b] D. Gryko, J. Li, J. R. Diers, K. M. Roth, D. F. Bocian, W. G. Kuhr, J. S. Lindsey, *J. Mater. Chem.* **2001**, *11*, 1162. [2c] T. Gross, F. Chevalier, J. S. Lindsey, *Inorg. Chem.* **2001**, *40*, 4762. [2d] K.-H. Schweikart, V. L. Malinovskii, J. R. Diers, A. A. Yasseri, D. F. Bocian, W. G. Kuhr, J. S. Lindsey, *J. Mater. Chem.* **2002**, *12*, 808. [2e] K.-H. Schweikart, V. L. Malinovskii, A. A. Yasseri, J. Li, A. B. Lysenko, D. F. Bocian, J. S. Lindsey, *Inorg. Chem.* **2003**, *42*, 7431. [2f] Z. Liu, A. A. Yasseri, J. S. Lindsey, D. F. Bocian, *Science* **2003**, *302*, 1543. [2g] L. Wei, K. Padmaja, W. J. Youngblood, A. B. Lysenko, J. S. Lindsey, D. F. Bocian, *J. Org. Chem.* **2004**, *69*, 1461.

[3] [3a] M. Lachkar, A. De Cian, J. Fischer, R. Weiss, *Inorg. Chem.* **1986**, *25*, 2107. [3b] D. Chabach, M. Lachkar, A. De Cian, J. Fischer, R. Weiss, *New J. Chem.* **1992**, *16*, 431. [3c] T.-H. Tran-Thi, T. A. Mattioli, D. Chabach, A. De Cian, R. Weiss, *J. Phys. Chem.* **1994**, *98*, 8279. [3d] D. Chabach, A. De Cian, J. Fischer, R. Weiss, M. El Malouli Bibout, *Angew. Chem. Int. Ed. Engl.* **1996**, *35*, 898.

[4] [4a] J. Jiang, R. L. C. Lau, T. W. D. Chan, T. C. W. Mak, D. K. P. Ng, *Inorg. Chim. Acta* **1997**, *255*, 59. [4b] J. Jiang, W. Liu, W.-F. Law, D. K. P. Ng, *Inorg. Chim. Acta* **1998**, *268*, 49. [4c] D. P. Arnold, J. Jiang, *Chem. Lett.* **1999**, 483. [4d] J. Jiang, Y. Bian, F. Furuya, W. Liu, M. T. M. Choi, N. Kobayashi, H.-W. Li, Q. Yang, T. C. W. Mak, D. K. P. Ng, *Chem. Eur. J.* **2001**, *7*, 5059. [4e] N. Pan, J. Jiang, X. Cui, D. P. Arnold, *J. Porphyrins Phthalocyanines* **2002**, *6*, 347. [4f] X. Sun, X. Xui, D. P. Arnold, M. T. M. Choi, D. K. P. Ng, J. Jiang, *Eur. J. Inorg. Chem.* **2003**, 1555.

[5] [5a] M. J. Stillman, T. Nyokong, in *Phthalocyanines − Properties and Applications*, vol. 1 (Eds.: C. C. Leznoff, A. B. P. Lever), VCH, New York, **1989**, pp. 133−290. [5b]E. Orti, J. L. Bredas, *J. Chem. Phys.* **1990**, *92*, 1228. [5c] R. Rousseau, R. Aroca, M. L. Rodriguez-Mendez, *J. Mol. Struct.* **1995**, *356*, 49. [5d] N. Ishikawa, *J. Porphyrins Phthalocyanines* **2001**, *5*, 87.

[6] [6a] J. Jiang, D. P. Arnold, H. Yu, *Polyhedron* **1999**, *18*, 2129. [6b] F. Lu, M. Bao, C. Ma, X. Zhang, D. P. Arnold, J. Jiang, *Spectrochim. Acta A* **2003**, *59*, 3273. [6c] M. Bao, N. Pan, C. Ma, D. P. Arnold, J. Jiang, *Vib. Spectrosc.* **2003**, *32*, 175.

[7] D. Chabach, A. De Cian, J. Fischer, R. Weiss, M. El Malouli Bibout, *Angew. Chem. Int. Ed. Engl.* **1996**, *35*, 898.

[8] D. Chabach, M. Lachkar, A. De Cian, J. Fischer, R. Weiss, *New J. Chem.* **1992**, *16*, 431.

[9] M. Moussavi, A. De Cian, J. Fischer, R. Weiss, *Inorg. Chem.* **1986**, *25*, 2107.

[10] J.-H. Fuhrhop, K. M. Kadish, D. G. Davis, *J. Am. Chem. Soc.* **1973**, *95*, 5140.

[11] F. Lu, X. Sun, R. Li, D. Liang, P. Zhu, C.-F. Choi, D. K. P. Ng, T. Fukuda, N. Kobayashi, M. Bai, C. Ma, J. Jiang, *New J. Chem.*, accepted.

[12] *SMART* and *SAINT* for Windows NT Software Reference Manuals, Version 5.0, Bruker Analytical X-ray Systems, Madison, WI, **1997**.

[13] G. M. Sheldrick, *SADABS − A Software for Empirical Absorption Correction*, University of Göttingen, Germany, **1997**.

[14] *SHELXL*, Reference Manual, Version 5.1, Bruker Analytical X-ray Systems, Madison, WI, **1997**.

Received April 8, 2004
Early View Article
Published Online July 29, 2004

  